Ms Thapanee Bangjang[1,2], Dr Nikolay Cherkasov[2 *], Dr Petr Denissenko[2], Dr Attasak Jaree[1,3], and Prof Evgeny Rebrov[2,4 *]

Enhanced droplet size control in liquid-liquid emulsions obtained in a wire-guided X-mixer

Abstract

A simple and efficient method has been proposed to control the droplet size in a liquid-liquid emulsion. Placing a metal wire along the centerline of an X-mixer completely changes the droplet formation mechanism. Droplets gradually form when flowing along the wire with droplet separation occurring at the tip of the wire rather than at the channel intersection in the X-mixer. The droplet size is now defined by the Plateau-Rayleigh instability developing in the axisymmetric annular flow region rather than by a sophisticated and hardly predictable 3-dimensional flow at the channel intersection. The wire-guided droplet formation allows for fine control of the droplet size by changing the wire diameter, position of the wire tip, and the flow rates. Further control of the droplet size can be achieved by adjusting the surface tension by addition of a surfactant.

Keywords: droplet; emulsion; microfluidics; microemulsion; X-mixer

Affiliations:

[1] Department of Chemical Engineering, Faculty of Engineering, Kasetsart University, Bangkok, Thailand 10900

[2] School of Engineering, University of Warwick, Coventry, CV4 7AL, United Kingdom

[3] Center for Advanced Studies in Industrial Technology, Faculty of Engineering, Kasetsart University, Bangkok, Thailand 10900

[4] Department of Biotechnology and Chemistry, Tver State Technical University, 170026, Nab. A. Nikitina 22, Russia

* corresponding authors: email: n.cherkasov@warwick.ac.uk, e.rebrov@warwick.ac.uk

1. Introduction

Emulsions with micron-size water-in-oil droplets, often referred to as microemulsions, are widely used in material synthesis, catalysis, diagnostics, drug delivery and analytical applications [1,2]. The microemulsion synthesis and their application in microfluidic devices decrease material consumption, enable processing in small volumes with low capital costs and in a high-throughput manner [3]. The continuous flow mode allows for the synthesis of chemically uniform catalyst particles that are more active and selective as compared to their counterparts obtained in batch [4]. It also allows obtaining stable microparticles for efficient drug delivery [5,6] as well as novel materials for chemical, food, oil and many other industries [7–9].

The efficient use of microemulsions requires precise control of the mean droplet diameter and the diameter distribution. In the food industry applications, long shelf life and fine texture can be achieved with a droplet size below 5 μm [7,10]. In energy applications, the droplet size distribution of a blended fuel affects the emulsion stability, viscosity, and hence the engine performance [11]. In medical and pharmaceutical applications, the droplet size determines transport rates of nutrients and oxygen.

The droplet size distribution depends on the particular mechanism of droplet generation and the geometry of the mixing device. A conventional method of bulk emulsification involves application of a high-shear stirrer to double phase mixtures. A broad droplet size distribution results from the stochastic nature of droplet generation [12,13]. Membrane emulsification provides a better control over the droplet size distribution and good control via the membrane pore size, properties of the liquids, and their flow rates [14]. The membranes with small and uniform pore dimensions are required, which results in high costs and a possibility of the membrane clogging [15]. Although the membrane emulsification is simple and easily scalable, the droplets generated have a typical relative standard deviation (RSD) at the level of 10-30% which is often insufficient [16,17].

An alternative set of the emulsion generation methods involves microfluidic devices that can improve droplet size uniformity. A number of geometries were used such as co-axial, T-, and X-mixers [18]. Montillet et al. [15] studied the formation of water-in-oil droplets using X- and T- mixers and obtained the droplets of about 5 μm in diameter with an RSD of 13-70 % depending on the amount of surfactant added. used efficient and widely An flow-focusing approach involves squeezing the flowing dispersed phase with two streams of continuous phase joining from opposite directions at an orifice [19]. Using this approach, an RSD can be reduced to below 5% [20]. Utada et al. (2007) investigated liquid-liquid flow regimes in a capillary flow-focusing device and found that the jetting regime results in non-uniform droplets due to the formation of small satellite droplets. The satellite droplet formation can be minimized using three-dimensional flow-focusing devices to obtain submicron emulsions [22]. Bauer et al. [23] demonstrated that

the surface modification of the walls allows for the efficient formation of single and double emulsions with an RSD below 1 %.

Despite advances in numbering up microfluidic devices above a kilogram per hour throughput, many microfluidic approaches require complex mixer geometries [24] and fabrication methods with micron tolerances [25–27]. Temperature variation can also have an effect on the emulsion dimensions but the effect is limited [28]. Placing a wire inside an available X mixer provides a cost-efficient yet powerful method to improve the droplet uniformity and gain control over droplet size. In this paper, the effect of the wire position and diameter, liquid flow rate, and the presence of surfactant on the droplet size and droplet size distribution is studied.

2. Experimental

A model ethanol and tetradecane system was studied considering applications in fuel blending (Supplementary material, S1). Ethanol and tetradecane are partially miscible at room temperature [29]. Tetradecane (further referred to as oil) should be addressed more correctly as a saturated solution of ethanol in tetradecane. The saturated ethanol and tetradecane solutions, however, are immiscible making the study applicable to other immiscible fluids such as water and mineral oil.

2.1. Materials

Tetradecane (99 %, VWR) and anhydrous ethanol (99 %, Fischer) were used as continuous and dispersed liquid phase respectively. For the visualization, Methylene blue dye (95 %, Sigma Aldrich) was added to ethanol at a concentration of 0.1 %. Tungsten wires (99.9 %, Advent Research Materials) with different diameter were used as guiding wires. The tungsten was selected for its high tensile strength and the high chemical resistance. Glycerol monostearate, named as biodiesel thereafter (99 %, Kao Corporation) was used as a surfactant.

2.2. Droplet generation

The mixing unit (Fig. 1) consists of standard 1/16" PEEK IDEX fluidic connectors: a T-mixer connected to an X-mixer. The tungsten wire was inserted along the axis of the mixer. The droplet generation was performed in a fluorinated ethylene propylene (FEP) tubing with an inner diameter of 500 μm and an outer diameter of 1.55 mm. Oil and ethanol were fed separately with two syringe pumps (neMESYS) equipped with 1.0 mL SGE precision syringes. The oil flow was fed via the side ports of the X-mixer using two tubes with an inner diameter of 100 μm for the uniform distribution of the flows [30–32]. The distance between the tip of the wire and the center of the X-mixer is denoted as the wire position.

Figure 1.

Optical images were recorded at 100 frames per second with a PointGrey camera connected to an optical microscope Olympus SZX16. The images of at least 100 droplets were recorded at each flow regime, and the droplet dimensions were measured using the ImageJ software [33]. The observed droplet shape was distorted by the light refraction in the circular tubing [34,35], hence the spherical droplets appeared elliptical (Fig. 2). This was concluded from the fact that when the droplets were introduced into a chip with a flat channel of 1 mm width where no optical distortions were expected, the droplets immediately appeared spherical with the same diameter as the minor axis of the elliptical droplets observed through the FEP tube. Therefore, the small axis of the ellipses in droplet images was taken as the droplet size.

3. Results

3.1. Effect of wire position

A series of experiments was carried out to compare the wire-guided and conventional droplet generation methods. The ethanol in oil droplets formed in the X-mixer)Fig. 2a) were compared with the droplets generated in the same mixer with a wire of 80 μm in diameter inserted along the centerline)Fig. 2b). The droplet size and the RSD obtained in the presence of the wire)328.1 ± 5.7) were smaller than those from the conventional X-mixer (473.8 ± 7.6 μm) obtained at the same flow rates.

Figure 2.

The effect of wire length beyond the center of the X-mixer is shown in Fig. 3. The average droplet size decreased with increasing the wire length up to 24 mm and then remained constant. In the subsequent experiments, the tip of the wire was positioned at a distance of 24 mm.

Figure 3.

3.2. Effect of the ethanol flow rate

A series of experiments was performed to study the effect of the dispersed phase flow rate because it has a major influence on the droplet size [2,36,37]. In these experiments, the oil flow rate was kept constant at 50 μL min^{-1} and the ethanol flow rate was varied from 2 to 10 μL min^{-1}. Characteristic images of the droplets obtained under different flow conditions are shown in Fig. 4.

Figure 4.

In the presence of the 80 μm wire, the smallest droplets were generated at an ethanol flow rate of 2 μL min^{-1}. A non-monotonous dependence of the droplet size on the ethanol flow rate was found in the mixer without the wire in contrast to the mixer with the wire, as shown in Tab. 1 and Fig. 4. It should be mentioned that the droplets obtained at the ethanol flow rate of 10 μm in the presence of the wire are more uniform in size with a twice lower RSD compared to the droplets formed in the conventional X-mixer.

Table 1.

3.3. Effect of the wire diameter and surfactant

The influence of the wire diameter on the droplet size has been studied in experiments with the wire diameters of 40, 80, 125 and 200 μm. A significant effect of the wire diameter on the droplet size was observed, as shown in Fig. 5a. A thick wire with a diameter of 200 μm at the ethanol flow rates of 2.0 and 10 $\mu L\ min^{-1}$ resulted in virtually the same droplets sizes as in case of the mixer without any wire. The droplet size decreases with the decreasing wire diameter from 200 to 80 μm and stays nearly constant when the wire diameter was further reduced from 80 to 40 μm (Fig. 5b).

Figure 5.

Fig. 5a shows that ethanol flows along the wire as semi-separate droplets, which indicates the essential role of surface phenomena in the wire-guided droplet generation. Instability of the annular flow along the wire, which resulted in the formation of ethanol layer with a non-uniform thickness, is inherently dependent on the surface tension between liquid phases. Therefore, the effect of the surfactant addition to the ethanol phase has been studied. A surfactant with the hydrophilic-lipophilic balance in the range of 3-6 tends to form water-in-oil emulsions, while that in the range of 7-10 tends to form foams or oil-in-water emulsions [38]. In the present study, glycerol monostearate (GMS) was chosen as a surfactant due to its optimal balance value of 3.8 to stabilize an ethanol in oil emulsion.

Fig. 6a shows characteristic images of droplets obtained at different surfactant concentrations in the presence of an 80 μm wire. Note that the shape of the interface between oil and water becomes less regular as the surface tension decreases. The droplet size decreased from 280 to 230 μm with the increasing surfactant concentration from 1.0 to 4.0 wt%. The droplet size obtained in the presence of 2 wt% GMS was smaller than that in the absence of the surfactant. Fig. 6b shows that the addition of 4 wt% GMS increased the RSD from 2 to 7%.

Figure 6.

4. Discussion

The droplet formation in T- and X-mixers is well studied in the literature. The main droplet formation mechanisms are pinching and jetting of the dispersed phase [16–18,39–44]. In the jetting mode, dispersed phase forms the elongated fluid body (jet), which becomes unstable and splits into separate droplets. In the pinching mode, droplets form one by one and, because the process is highly dynamic [45], smaller satellite droplets are often formed making the obtained emulsion less uniform [46].

In traditional x-mixers, the pinching takes place. In our case the Weber number, which describes the pinching to jetting transition around a value of 1, was below 10^{-3} confirming that the droplets were formed by pinching [21]. The pinching mechanism agrees with very low capillary numbers, below 10^{-6} for the dispersed phase, and a Reynolds number close to 1 for both continuous and dispersed phases [18,42,44]. Moreover, a uniform size of the droplets formed with an RSD below 3% also indicates the absence of jetting where much lower droplet uniformity is expected. It is worth noting that in the flow around the wire inertial effects can be neglected everywhere except inside the X-mixer and at the droplet pinching point at the wire tip. As discussed below, however, flow at both locations has little influence on the droplet size.

Introduction of the guiding wire totally changes the mechanism of the droplet formation. As presented in Fig. 7a, instead of pinching into droplets at the X-mixer intersection, ethanol flows around the wire. The uniform layer of ethanol becomes unstable, starts to separate, and form bulges similarly to what happens in jetting regimes. When the bulges of ethanol reach the end of the wire, they pinch off as droplets. Now, instead of a 3-dimensional pinching off process at the X-point of the mixer, the droplet formation is defined by a slow evolution of an annular flow along the wire.

Figure 7.

The behavior of the annular flow, in this case, is described by the Plateau-Rayleigh instability [46] as any liquid interface tends to minimize its area. In the case of cylindrical bodies of liquid, the instability leads to formation of waves in the axial direction, necking, and eventual breakup of a liquid bridge into droplets. More exactly, the capillary pressure created by the interface in necks (which is higher than that in the bulges) pushes ethanol further from necks into the bulges. Such pushing provides positive feedback and increases the instability.

The Plateau-Rayleigh instability occurs in liquid bridges when their length exceeds circumference which also defines the minimum wavelength of the instability [48]. In our case, existence of the wire prevents complete splitting of the bulges into separate droplets making them traveling downstream until the wire tip. The increasing instability wavelength explains the growth of the droplet size with the wire diameter and with the ethanol flow rate observed experimentally in Fig. 5 and Tab. 1.

The bulging of the inner fluid has been modeled by assuming that the bulge period is equal to the interface circumference (Plateau-Rayleigh limit). Dashed lines in Fig. 5b show the model predictions obtained by solving the axisymmetric Navier-Stokes conditions as described in the Supporting Information, S2. The overall trend of increasing droplet size with the wire diameter is explained well by the model, but the discrepancy with the experiment, however, is large. We explain the discrepancy by the changing ethanol amount in the bulges along the wire length. Fig. 7b illustrates the phenomena: The thickness of necks decreases downstream and affects the flow of ethanol through them. This phenomenon can be seen clearly

when the frame of reference is changed to that moving with the bulge top highlighted with the red arrow in Fig. 7c. In the new frame of reference, the inflow of ethanol towards the bulge is lower than the outflow. This decreases the amount of fluid in bulges and hence the droplet size. Hence, as the instability grows along the wire the volume of fluid contained in the forming bulges (droplets-to-be) reduces, in agreement with the experiment (Fig. 3). When the necks are reduced to the diameter of the wire, the flow between bulges ceases hence the droplet size remains constant onwards in agreement with the Fig. 3.

5. Conclusions

The droplet generation has been investigated in the wire-guided X-mixer. This simple yet powerful tool enables the fine control of the size of droplets formed in liquid-liquid flows and makes the droplet size distribution narrower. The droplets in the range of 250-450 μm with an RSD below 2 % have been obtained in a circular tube of 500 μm diameter. The droplet size is defined by the capillary-driven Plateau-Rayleigh instability of the two-layered annular flow in the gap between the guiding wire and the tube walls. The slow nature of droplet formation, different from that related to breakup in a conventional X-mixer, provides the possibility for fine control of the droplet size by altering the tip position of the guiding wire.

Acknowledgments

The authors acknowledge the financial support from the Thailand Research Fund through the Royal Golden Jubilee Ph.D. Program)Grant No. PHD/0243/2553) and the Russian Science Foundation project 15-13-20015. We are also grateful to Md. Taifur Rahman for the preliminary experiments which were not included in this publication.

Conflict of Interest

The authors declare no conflict of interest.

Funding

The work was funded by the Thailand Research Fund through the Royal Golden Jubilee Ph.D. Program)Grant No. PHD/0243/2553) and the Russian Science Foundation project 15-13-20015.

Symbols used

d	[m]	diameter

References

[1] W. L. Chou, P. Y. Lee, C. L. Yang, W. Y. Huang, Y. S. Lin, *Micromachines*. **2015**, *6* (9), 1249–1271. DOI: 10.3390/mi6091249.

[2] S.-Y. Teh, R. Lin, L.-H. Hung, A. P. Lee, *Lab Chip*. **2008**, *8* (2), 198–220. DOI: 10.1039/b715524g.

[3] A. Huebner, S. Sharma, M. Srisa-Art, F. Hollfelder, J. B. Edel, A. J. deMello, *Lab Chip*. **2008**, *8* (8), 1244. DOI: 10.1039/b806405a.

[4] M. Boutonnet, M. Sanchez-Dominguez, *Catal. Today*. **2017**, *285*, 89–103. DOI: 10.1016/j.cattod.2016.12.047.

[5] W. Zhu, C. Guo, A. Yu, Y. Gao, F. Cao, G. Zhai, *Int. J. Pharm.* **2009**, *378* (1–2), 152–158. DOI: 10.1016/j.ijpharm.2009.05.019.

[6] H. Chen, X. Chang, D. Du, J. Li, H. Xu, X. Yang, *Int. J. Pharm.* **2006**, *315* (1–2), 52–58. DOI: 10.1016/j.aca.2005.10.016.

[7] A. A. Maan, A. Nazir, M. K. I. Khan, R. Boom, K. Schroen, *J. Food Eng.* **2015**, *147*, 1–7. DOI: 10.1016/j.jfoodeng.2014.09.021.

[8] A. Bera, T. Kumar, K. Ojha, A. Mandal, *Fuel*. **2014**, *121*, 198–207. DOI: 10.1016/j.fuel.2013.12.051.

[9] P. Lisk, E. Bonnot, M. T. Rahman, R. Pollard, R. Bowman, V. Degirmenci, E. V. Rebrov, *Chem. Eng. J.* **2016**, *306*, 352–361. DOI: 10.1016/j.cej.2016.07.059.

[10] J. Floury, A. Desrumaux, J. Lardières, *Innov. Food Sci. Emerg. Technol.* **2000**, *1* (2), 127–134. DOI: 10.1016/S1466-8564(00)00012-6.

[11] N. Arpornpong, C. Attaphong, A. Charoensaeng, D. A. Sabatini, S. Khaodhiar, *Fuel*. **2014**, *132*, 101–106. DOI: 10.1016/j.fuel.2014.04.068.

[12] R. Foudazi, S. Qavi, I. Masalova, A. Y. Malkin, *Adv. Colloid Interface Sci.* **2015**, *220*, 78–91. DOI: 10.1016/j.cis.2015.03.002.

[13] J. S. Sander, A. R. Studart, R. Studart, *Soft Matter*. **2014**, *10* (1), 60–68. DOI: 10.1039/C3SM51900G.

[14] S. M. Joscelyne, G. Trägårdh, *J. Memb. Sci.* **2000**, *169* (1), 107–117. DOI: 10.1016/S0376-7388(99)00334-8.

[15] A. Montillet, S. Nedjar, M. Tazerout, *Fuel*. **2013**, *106*, 410–416. DOI: 10.1016/j.fuel.2012.11.018.

[16] S. R. Kosvintsev, G. Gasparini, R. G. Holdich, *J. Memb. Sci.* **2008**, *313* (1–2), 182–189. DOI: 10.1016/j.memsci.2008.01.009.

[17] E. Egidi, G. Gasparini, R. G. Holdich, G. T. Vladisavljević, S. R. Kosvintsev, *J. Memb. Sci.* **2008**, *323* (2), 414–420. DOI: 10.1016/j.memsci.2008.06.047.

[18] C. N. Baroud, F. Gallaire, R. Dangla, *Lab Chip*. **2010**, *10* (16), 2032–2045. DOI: 10.1039/c001191f.

[19] S. L. Anna, N. Bontoux, H. A. Stone, *Appl. Phys. Lett.* **2003**, *82* (3), 364–366. DOI: 10.1063/1.1537519.

[20] P. Zhu, L. Wang, *Lab Chip*. **2017**, *17* (1), 34–75. DOI: 10.1039/C6LC01018K.

[21] A. S. Utada, A. Fernandez-Nieves, H. A. Stone, D. A. Weitz, *Phys. Rev. Lett.* **2007**, *99* (9), 1–4. DOI: 10.1103/PhysRevLett.99.094502.

[22] W.-C. Jeong, J.-M. Lim, J.-H. Choi, J.-H. Kim, Y.-J. Lee, S.-H. Kim, G. Lee, J.-D. Kim, G.-R. Yi, S.-M. Yang, *Lab Chip*. **2012**, *12* (8), 1446–1453. DOI: 10.1039/c2lc00018k.

[23] W.-A. C. Bauer, M. Fischlechner, C. Abell, W. T. S. Huck, *Lab Chip*. **2010**, *10* (14), 1814–1819. DOI: 10.1039/c004046k.

[24] N.-N. Deng, S.-X. Sun, W. Wang, X.-J. Ju, R. Xie, L.-Y. Chu, *Lab Chip*. **2013**, *13* (18), 3653–3657. DOI: 10.1039/c3lc50533b.

[25] T. Nisisako, T. Torii, *Lab Chip*. **2008**, *8* (2), 287–293. DOI: 10.1039/B713141K.

[26] H.-H. Jeong, V. R. Yelleswarapu, S. Yadavali, D. Issadore, D. Lee, *Lab Chip*. **2015**, *15* (23), 4387–4392. DOI: 10.1039/C5LC01025J.

[27] D. Conchouso, D. Castro, S. A. Khan, I. G. Foulds, *Lab Chip*. **2014**, *14* (16), 3011–3020. DOI: 10.1039/C4LC00379A.

[28] C. Malafosse, J. Blanco, N. le Sauze, K. Loubière, J. Ollagnier, H. Rolland, A. Pierre, L. Prat, Chem. Eng. Technol. **2018**, 41, 1965-1974. DOI: 10.1002/ceat.201800063.

[29] H. Matsuda, K. Ochi, *Fluid Phase Equilib.* **2004**, *224* (1), 31–37. DOI: 10.1016/J.FLUID.2004.05.006.

[30] M. Al-Rawashdeh, L. J. M. Fluitsma, T. A. Nijhuis, E. V. Rebrov, V. Hessel, J. C. Schouten, *Chem. Eng. J.* **2012**, *181–182*, 549–556. DOI: 10.1016/j.cej.2011.11.086.

[31] M. Al-Rawashdeh, F. Yue, N. G. Patil, T. A. Nijhuis, V. Hessel, J. C. Schouten, E. V. Rebrov, *AIChE J.* **2014**, *60* (5), 1941–1952. DOI: 10.1002/aic.14443.

[32] Y. Su, K. Kuijpers, V. Hessel, T. Noël, *React. Chem. Eng.* **2016**, *1* (1), 73–81. DOI: 10.1039/C5RE00021A.

[33] C. A. Schneider, W. S. Rasband, K. W. Eliceiri, *Nat. Methods*. **2012**, *9* (7), 671–675. DOI: 10.1038/nmeth.2089.

[34] M. L. Lowe, P. H. Kutt, *Exp. Fluids*. **1992**, *13*, 315–320. DOI: 10.1007/bf00206543.

[35] R. Budwig, *Exp. Fluids*. **1994**, *17*, 350–355.

[36] T. Nisisako, T. Torii, T. Higuchi, *Lab Chip*. **2002**, *2* (1), 24–26. DOI: 10.1039/B108740C.

[37] P. Tabeling, *Lab Chip*. **2009**, *9* (17), 2428–2436. DOI: 10.1039/b904937c.

[38] P. Tabeling, *Introduction to Microfluidics*, Oxford University Press **2005**.

[39] Y. Lu, T. Fu, C. Zhu, Y. Ma, H. Z. Li, *Microfluid. Nanofluidics*. **2014**, *16* (6), 1047–1055. DOI: 10.1007/s10404-013-1274-x.

[40] T. Fu, Y. Ma, D. Funfschilling, H. Z. Li, *Chem. Eng. Sci.* **2009**, *64* (10), 2392–2400. DOI: 10.1016/j.ces.2009.02.022.

[41] V. van Steijn, M. T. Kreutzer, C. R. Kleijn, *Chem. Eng. Sci.* **2007**, *62* (24), 7505–7514. DOI: 10.1016/j.ces.2007.08.068.

[42] C. X. Zhao, A. P. J. Middelberg, *Chem. Eng. Sci.* **2011**, *66* (7), 1394–1411. DOI: 10.1016/j.ces.2010.08.038.

[43] Z. Z. Chong, S. H. Tan, A. M. Gañán-Calvo, S. B. Tor, N. H. Loh, N.-T. Nguyen, *Lab Chip*. **2016**, *16* (1), 35–58. DOI: 10.1039/C5LC01012H.

[44] H. Huang, X. He, *Lab Chip*. **2015**, *15* (21), 4197–4205. DOI: 10.1039/C5LC00730E.

[45] P. Garstecki, M. J. Fuerstman, H. A. Stone, G. M. Whitesides, *Lab Chip*. **2006**, *6* (3), 437–446. DOI: 10.1039/b510841a.

[46] V. Cristini, Y.-C. Tan, *Lab Chip*. **2004**, *4* (4), 257–264. DOI: 10.1039/B403226H.

[47] L. Rayleigh, *Proc. R. Soc. London*. **1879**, *29* (196–199), 71–97. DOI: 10.1098/rspl.1879.0015.

[48] S. Atreya, P. H. Steen, *Proc. R. Soc. A Math. Phys. Eng. Sci.* **2002**, *458* (2027), 2645–2669. DOI: 10.1098/rspa.2002.0989.

Tables with Headings

Table 1. The size of the droplets formed in the X-mixer in with the 80 μm (d_{wire}) and without the wire ($d_{no\ wire}$) and their relative standard deviations (RSD). The oil flow rate is 50 μL min^{-1}.

Ethanol flow rate)μL min^{-1}(	d_{wire} (μm)	RSD_{wire} (%)	$d_{no\ wire}$ (μm)	$RSD_{no\ wire}$ (%)
2.0	283.2 ± 5.8	2.0	402.2 ± 6.6	1.6
5.0	328.1 ± 5.7	1.7	473.8 ± 7.6	1.6
10.0	359.0 ± 4.5	1.3	404.6 ± 9.6	2.4

Figure legends

Figure 1. A photograph of the mixing unit used. The centerline white line highlights the location of the wire.

Figure 2. Ethanol droplet size distribution obtained in (a) an X-mixer and (b) the same mixer with an 80 μm wire inserted at the flow

Figure 3. Effect of the 80 μm wire tip position on the average droplet size obtained in the X-mixer at the flow rates of 5 μL min^{-1} for ethanol and 50 μL min^{-1} for oil.

Figure 4. Optical images of the ethanol droplets formed in the X-mixer (a-c) with the 80 μm wire and (d-f) without the wire at the flow rates of 50 μL min^{-1} for oil and (a, d) 2, (b, e) 5, or (c, f) 10 μL min^{-1} for ethanol.

Figure 5. (a) Images of ethanol droplets formed in the wire-guided X-mixer with wires of different diameters at the flow rates of 5 μL min^{-1} for ethanol and 50 μL min^{-1} for oil. (b) The droplets size as a function of the wire diameter. The dashed lines show the droplet sizes formed without the wire; the dotted line corresponds to the Plateau-Rayleigh stability model.

Figure 6. (a) Optical images of ethanol droplets formed in the wire-guided X-mixer at the flow rates of 5 μL min^{-1} for ethanol and 50 μL min^{-1} for oil and (b) the droplet size as a function of the surfactant concentration.

Figure 7. Droplet formation and growth in the presence of the wire. The zoomed-in region uses (b) the wire or (b) the bulge (red dot) as a frame of reference. More inner fluid is leaving the droplet through the bigger trailing neck than entering through the smaller leading neck as shown by red vectors of fluid velocity.

Table of Contents

A simple and efficient method has been proposed to control the droplet size in a liquid-liquid emulsion. Placing a metal wire along the centerline of the X-mixer changes the droplet formation mechanism. The wire improves droplet uniformity and provides an additional control over the droplet size via the wire diameter, position of the wire tip.

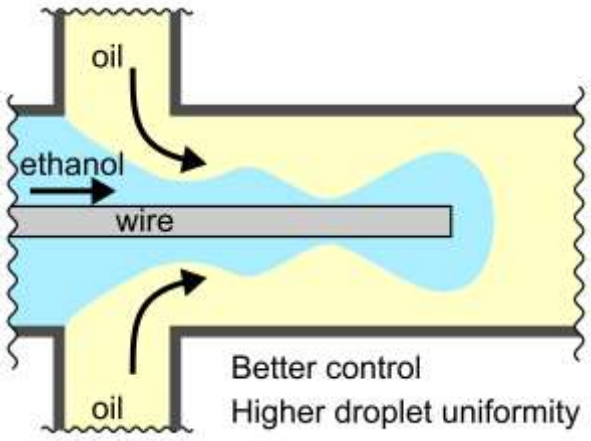

Supporting Information

S1. Comparison of physical properties of tetradecane and diesel

Ethanol and tetradecane were selected to model the ethanol-diesel system that is widely used in by blending renewable ethanol to diesel fuels. Tetradecane has the main parameters relevant to the droplet formation comparable to that of diesel. Compared to water, ethanol has a much lower surface tension and provides more difficult emulsification. However, the section that describes the effect of surfactant in the paper demonstrates that the findings can be generalized to the water-in-oil systems using a small amount of surfactant.

Table S1. Key properties of liquids studied.

Components	Dynamic viscosity)mPa s(	Surface tension)mN m^{-1}(
Tetradecane	2.3	26.0
Diesel	3.0	29.3
Ethanol	1.2	22.0
Water	0.9	72.0

S2. Derivation of axial profiles of fluid velocity

Consider an axisymmetric flow in the annular ring with the axis of symmetry aligned with z-axis. We assume the axial variation of the flow profile is much less than the radial variation. As a result, we can neglect axial derivatives $\frac{\partial}{\partial z}$ and assume radial velocity is zero. Now, the problem is reduced to that for the axial velocity U dependent on the radius r. The time-independent Navier-Stokes equations for the axisymmetric flow independent of axial coordinate are shown in Eq. (1):

$$\frac{1}{r}\frac{d}{dr}\left(\frac{1}{r}\frac{dU}{dr}\right)=\frac{1}{\mu}P_z. \tag{1}$$

Here, μ is the fluid dynamic viscosity and P_z is the axial pressure gradient. Denoting the flow velocity in ethanol (inner fluid) as U_i and the flow velocity in oil (outer fluid) as U_o, we obtain Eqs. (2, 3):

$$U_i=\frac{P_z}{4\mu_i}r^2+A_i\ln r+B_i, \tag{2}$$

$$U_o=\frac{P_z}{4\mu_o}r^2+A_o\ln r+B_o, \tag{3}$$

Where A and B are constants. Denoting the tube radius as R_o, wire radius as R_i, the liquid interface radius as R, and the flow rates of oil and ethanol as Q_o and Q_i, the non-slip conditions at the outer tube and at the wire result in Eqs. (4, 5):

$$0 = \frac{P_z}{4\mu_i} R_i^2 + A_i \ln R_i + B_i, \tag{4}$$

$$0 = \frac{P_z}{4\mu_o} R_o^2 + A_o \ln R_o + B_o, \tag{5}$$

Continuity of the fluid velocity at the interface provides Eq. (6):

$$\frac{P_z}{4\mu_i} R^2 + A_i \ln R + B_i = \frac{P_z}{4\mu_o} R^2 + A_o \ln R + B_o, \tag{6}$$

The condition on the equal the shear stress in the inner and outer parts of the flow at the interface results in Eq. (7):

$$\mu_i A_i = \mu_o A_o, \tag{7}$$

Integrating fluid velocities to get flow rates of inner and outer phases, we derive Eqs. (8, 9):

$$\frac{P_z}{12\mu_i}\left(R^3 - R_i^3\right) + A_i\left(R\ln R - R_i \ln R_i\right) + B_i\left(R - R_i\right) = Q_i, \tag{8}$$

$$\frac{P_z}{12\mu_o}\left(R_o^3 - R^3\right) + A_o\left(R_o \ln R_o - R\ln R\right) + B_o\left(R_o - R\right) = Q_o, \tag{9}$$

We therefore have 6 equations with the 6 unknowns: $R, P_z, A_i, B_i, A_o, B_o$.

Expressing B_i and B_o from Eqs. (4) and (5) and substituting to Eqs. (7), (8), (9), we derive a system of equations (10):

$$\begin{cases} \mu_i A_i = \mu_o A_o \\ \frac{P_z}{4\mu_i} R^2 + A_i \ln R + \frac{P_z}{4\mu_o} R_o^2 + A_o \ln R_o = \frac{P_z}{4\mu_o} R^2 + A_o \ln R + \frac{P_z}{4\mu_i} R_i^2 + A_i \ln R_i \\ \frac{P_z}{12\mu_i}\left(R^3 - R_i^3\right) + A_i\left(R\ln R - R_i \ln R_i\right) - \left(\frac{P_z}{4\mu_i} R_i^2 + A_i \ln R_i\right)\left(R - R_i\right) = Q_i \\ \frac{P_z}{12\mu_o}\left(R_o^3 - R^3\right) + A_o\left(R_o \ln R_o - R\ln R\right) - \left(\frac{P_z}{4\mu_o} R_o^2 + A_o \ln R_o\right)\left(R_o - R\right) = Q_o \end{cases}, \tag{10}$$

After elimination of the A_i, the system may be simplified to system (11):

$$\begin{cases} \frac{P_z}{4\mu_i}R^2+\frac{\mu_o}{\mu_i}A_o\ln R+\frac{P_z}{4\mu_o}R_o{}^2+A_o\ln R_o=\frac{P_z}{4\mu_o}R^2+A_o\ln R+\frac{P_z}{4\mu_i}R_i{}^2+\frac{\mu_o}{\mu_i}A_o\ln R_i \\ P_z\left(\frac{1}{12}R^3+\frac{1}{6}R_i{}^3-\frac{1}{4}R_i{}^2R\right)+A_o\mu_oR\ln\frac{R}{R_i}=\mu_iQ_i \\ P_z\left(\frac{1}{12}R^3+\frac{1}{6}R_o{}^3-\frac{1}{4}R_o{}^2R\right)+A_o\mu_oR\ln\frac{R}{R_0}=-\mu_oQ_o \end{cases}, \quad (11)$$

Factorizing the first equation and resolving the last two equations in P_z and A_o, we derive system (12)

$$\begin{cases} P_z\left(\mu_oR^2-\mu_iR^2-\mu_oR_i{}^2+\mu_iR_o{}^2\right)=4A_o\mu_o\left(\mu_i\ln\frac{R}{R_o}-\mu_o\ln\frac{R}{R_i}\right) \\ P_z=\left(\mu_oR\ln\frac{R}{R_0}\mu_iQ_i+\mu_oR\ln\frac{R}{R_i}\mu_oQ_o\right)/\Delta \\ A_o=\left(-\left(\frac{1}{12}R^3+\frac{1}{6}R_i{}^3-\frac{1}{4}R_i{}^2R\right)\mu_oQ_o-\left(\frac{1}{12}R^3+\frac{1}{6}R_o{}^3-\frac{1}{4}R_o{}^2R\right)\mu_iQ_i\right)/\Delta \end{cases}, \quad (12)$$

Here, $\Delta=\mu_oR\left(\left(\frac{1}{12}R^3+\frac{1}{6}R_i{}^3-\frac{1}{4}R_i{}^2R\right)\ln\frac{R}{R_0}-\left(\frac{1}{12}R^3+\frac{1}{6}R_o{}^3-\frac{1}{4}R_o{}^2R\right)\ln\frac{R}{R_i}\right)$

Substituting P_z and A_o to the first equation, we have the equation for interface radius R in Eq. (13).

$$R\left(\mu_iQ_i\ln\frac{R}{R_0}+\mu_oQ_o\ln\frac{R}{R_i}\right)\left(\mu_oR^2-\mu_iR^2-\mu_oR_i{}^2+\mu_iR_o{}^2\right)+$$
$$+4\left(\mu_oQ_o\left(\frac{1}{12}R^3+\frac{1}{6}R_i{}^3-\frac{1}{4}R_i{}^2R\right)+\mu_iQ_i\left(\frac{1}{12}R^3+\frac{1}{6}R_o{}^3-\frac{1}{4}R_o{}^2R\right)\right)\left(\mu_i\ln\frac{R}{R_o}-\mu_o\ln\frac{R}{R_i}\right)=0$$

(13)

Equation 13 was solved numerically in MATLAB. The diameter of the ethanol droplet (D) formed was calculated with Eq. (14):

$$D=\left(12R\cdot\pi\left(R^2-R_i^2\right)\right)^{1/3}. \quad (14)$$